NANO
LETTERS

Optical and Magnetic Properties of Hexagonal Arrays of Subwavelength Holes in Optically Thin Cobalt Films

G. Ctistis,[*,†,⊥] **E. Papaioannou,**[‡,§] **P. Patoka,**[†] **J. Gutek,**[†] **P. Fumagalli,**[‡] and **M. Giersig**[†,‖]

Center of Advanced European Studies and Research, Nanoparticle Technology Department, 53175 Bonn, Germany, Institut für Experimentalphysik, Freie Universität Berlin, 14195 Berlin, Germany, Department of Physics and Materials Science, Uppsala University, 75121 Uppsala, Sweden, Helmholtz-Zentrum Berlin für Materialien und Energie GmbH, 14109 Berlin, Germany, and FOM Institute for Atomic and Molecular Physics (AMOLF), 1098 SJ Amsterdam, The Netherlands

ABSTRACT

In this study, we present our experimental results on the optical, magnetic, as well as magneto-optic properties of hexagonal arrays of subwavelength holes in optically thin cobalt films. Different meshes were used with hole diameters ranging between 220 and 330 nm while the interhole distance has been kept constant at 470 nm. The hole pattern modifies completely the magnetic behavior of the cobalt films; it gives rise to an increase of the coercive field of the in-plane magnetization with increasing hole diameter and to the appearance of out-of-plane magnetization components. Magneto-optic measurements show a spectacular magneto-optic response at wavelengths where surface plasmon-polaritons are supported by the structure as deduced in optical measurements. The experiments demonstrate the ability to artificially control the magnetic and thus the magneto-optic properties in hole array structures.

Surface plasmon-polariton (SPP) propagation along the interfaces of nanostructured metallic films has been studied extensively[1−28] throughout the last decades, being responsible for the observed special optical properties in these kind of materials. The studies focused on the noble metals due to the low absorption losses of the SPPs in these metals and due to their potential for possible applications in optoelectronics and biosensing. Although the effects should in principle be visible also in other metals, for example, in ferromagnets, only limited research has been done so far.[29−36] Since the excitation of SPPs is directly affected by the dielectric properties of the material and a magnetic field alters the permittivity tensor, a direct influence of the applied field to the SPP propagation should be visible. Yet, this influence, that is, the change of dispersion relation, would need very strong magnetic fields for metallic based SPPs.

* To whom correspondence should be addressed. E-mail: g.ctistis@amolf.nl.
† Center of Advanced European Studies and Research.
⊥ FOM Institute for Atomic and Molecular Physics (AMOLF).
‡ Freie Universität Berlin.
§ Uppsala University.
‖ Helmholtz-Zentrum Berlin für Materialien und Energie GmbH.

Because of the magneto-optic activity of ferromagnetic metals, the required external fields to observe such magneto-plasmonic effects should be low, although broadening due to absorption makes it difficult to observe any effect. For a uniaxial anisotropic material such as cobalt the permittivity tensor under an applied external field perpendicular to the surface takes the form

$$\varepsilon = \begin{pmatrix} \varepsilon_o & -i\varepsilon_o Q & 0 \\ i\varepsilon_o Q & \varepsilon_e & 0 \\ 0 & 0 & \varepsilon_e \end{pmatrix} \qquad (1)$$

where $\varepsilon_o = n_o^2$ and $\varepsilon_e = n_e^2$ are the ordinary and extraordinary refractive indices, and $Q = 0.0262 - 0.0058i$ denotes the magneto-optic Voigt constant for Co.[37] It is directly visible that the magnetic field alters the permittivity tensor and thus changes the optical behavior of the material leaving a possibility to influence the light propagation.

In this work, we will present our experimental results on the optical, magnetic, and magneto-optic properties of a hexagonal array of holes in optically thin cobalt films. We will show that the SPP excitation in the array indeed affects the transmission and reflection of light in the presence of an applied external field and that this magneto-optic effect is larger than for a control cobalt film of the same thickness. We will further investigate the magnetization reversal process as well as the domain formation for this array and compare it to micromagnetic simulations.

Experimental Section. The films under study were prepared using self-assembly nanosphere lithography.[38] As a mask template, we used negatively charged polystyrene (PS) latex spheres (diluted in water) with a diameter of 470 nm. These were dispersed in an ethanol−water solution and slowly applied to a water surface in a Petri dish using a micropipette. The floating PS-spheres reorient themselves on the water surface, forming a closed-packed hexagonal crystal, which is, over a large area, defect-free and only one monolayer in thickness. This crystal can afterward be deposited onto a clean substrate (in our case either sapphire or Si(111)) by slowly evaporating the water. Because the closed-packed structure avoids the growth of a closed metal film, the diameter of the spheres has been reduced by a reactive ion-etching procedure. Control of the etching parameters enables us to control the diameter of the PS-spheres after the process, resulting in diameters between 220 and 330 nm, respectively. The thus obtained structure served as a mask for the evaporation of the 50 and 100 nm thick cobalt films by means of molecular-beam epitaxy at a base pressure of 10^{-7} mbar. Thereafter, a chemical treatment dissolved the PS-spheres, leaving behind the metal film with a hexagonal array of holes (see Figure 1b).

All the conducted experiments were performed ex situ at room temperature. The samples were characterized with an UV−vis spectrometer (Cary5000, Varian), which was equipped with a home-build sample holder, allowing us to measure angle-dependent spectra in the wavelength range of 200−2500 nm (0.5−6.2 eV) and up to 30° incident angle (Figure 1a). The magneto-optic measurements were
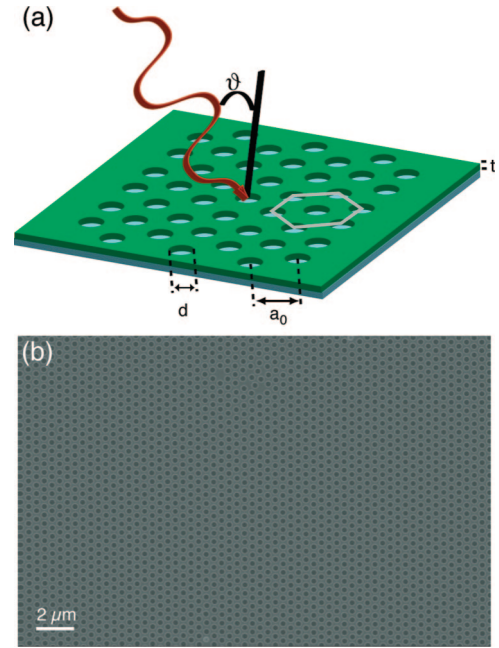

Figure 1. (a) Schematic representation of the hexagonal hole array in the cobalt film and the relevant dimensions for the measurement: thickness of the film t, diameter of the holes d, interhole distance a_0, and incident angle ϑ. (b) Scanning electron micrograph of the hole array showing a large area defect-free structure.

performed in an automated Kerr-spectrometer working in the polar geometry (incident angle 2.5°) with a resolution of 2 mdeg in the wavelength range of 240−1770 nm (0.7−5.1 eV) and an applied out-of-plane field of up to $B = 1.6$ T. Additionally, longitudinal hysteresis loops were recorded using laser sources at different wavelengths at room temperature and with applied in-plane fields of up to $B = 90$ mT. Further magnetic characterization of the cobalt samples was done in a magnetic-force microscope (MFM; Nanoscope, Veeco) with applied in- and out-of-plane external fields.

Results and Discussion. A typical zero-order transmission spectrum at normal incidence through the Co hole array is shown in Figure 2a (black circles) for a Co thickness of 50 nm and a hole diameter of 270 nm, while the lattice parameter of the array is 470 nm, respectively. The spectrum shows several transmission-band resonances, which are a result of the resonant coupling of the light to surface plasmon (SP) excitations of both interfaces. Since normal incident light impinging on a metal surface cannot excite surface plasmon excitations,[39] the periodicity of the array is necessary for the coupling. In this case, the conservation of momentum can be written as[39]

$$\vec{k}_{SP} = \vec{K}_0 \pm n\vec{b}_x \pm m\vec{b}_y \qquad (2)$$

where the in-plane component of the light wave-vector $\vec{k}_0$ is $\vec{K}_0 = (\omega/c)(\vec{k}_0/|\vec{k}_0|)\sin\vartheta$ and ω is the frequency, c is the speed of light, $\vec{b}_x$ and $\vec{b}_y$ are the reciprocal lattice vectors for the hexagonal lattice, ϑ is the incident angle, and n and m are integers. On the other hand, conservation of energy at the interface leads to[39]
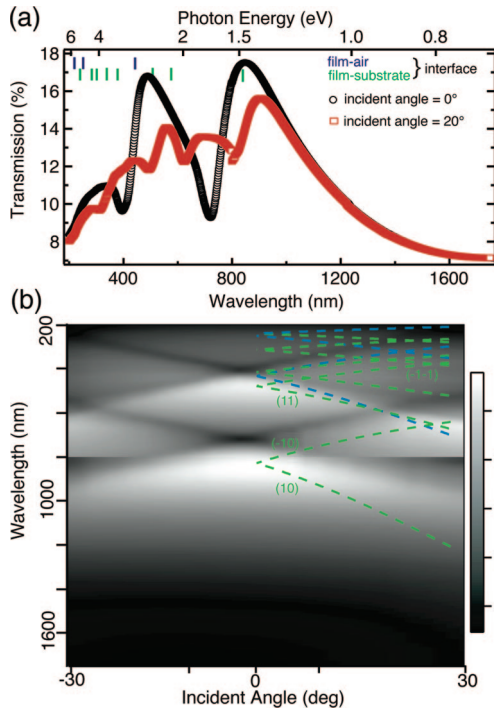
Figure 2. (a) Measured transmission spectra of a 50 nm thick Co film for two incident angles, that is, at normal incidence (black circles) and at 20° (red squares). The vertical lines denote the, with eq 5 calculated positions of transmission maxima for both interfaces at normal incidence, that is, film−substrate interface (green lines) and film-air interface (blue lines). (b) Angle dependent measurements along the Γ-K-direction of the hexagonal array. Additionally, the calculated dispersion of the different SP-modes is shown in the graph. The green lines denote the film−substrate SP-modes while the blue lines belong to film-air interfacial SP-modes.

$$|\vec{k}_{\mathrm{SP}}| = \frac{\omega}{c}\sqrt{\frac{\varepsilon_{\mathrm{m}}\varepsilon_{\mathrm{d}}}{\varepsilon_{\mathrm{m}} + \varepsilon_{\mathrm{d}}}} \quad (3)$$

with ε_{m} and ε_{d} as the real parts of the dielectric constants of the metal and the dielectric, respectively. Combining both equations leads to the desired dispersion relation, which in the case of a hexagonal lattice can be written as

$$|\vec{k}_{\mathrm{SP}}| = \sqrt{k_0^2 \sin^2 \vartheta \pm \frac{4\pi^2}{a_0^2}k_0(n+m)\sin \vartheta + \frac{4\pi^2}{a_0^2}\left(\frac{4}{3}(n^2 + m^2 + nm)\right)} \quad (4)$$

In case of normal incidence, eq 4 is reduced to the well-known equation

$$\lambda = \frac{a_0}{\sqrt{\frac{4}{3}(n^2 + m^2 + nm)}}\sqrt{\frac{\varepsilon_{\mathrm{m}}\varepsilon_{\mathrm{d}}}{\varepsilon_{\mathrm{m}} + \varepsilon_{\mathrm{d}}}} \quad (5)$$

with a_0 the periodicity of the array and the integers n and m denoting the order of the SP resonances. Since the light can penetrate the metal film quite well, we have to take both interfaces into account, that is, the air-metal and the metal-sapphire interfaces. The calculated positions of the expected maxima for normal incidence, which are represented by the blue (film-air-interface) and green (film−substrate-interface) vertical lines in Figure 2a, are in good agreement with the measured transmission maxima, thus explaining the spectral features as SP modes of the involved interfaces.
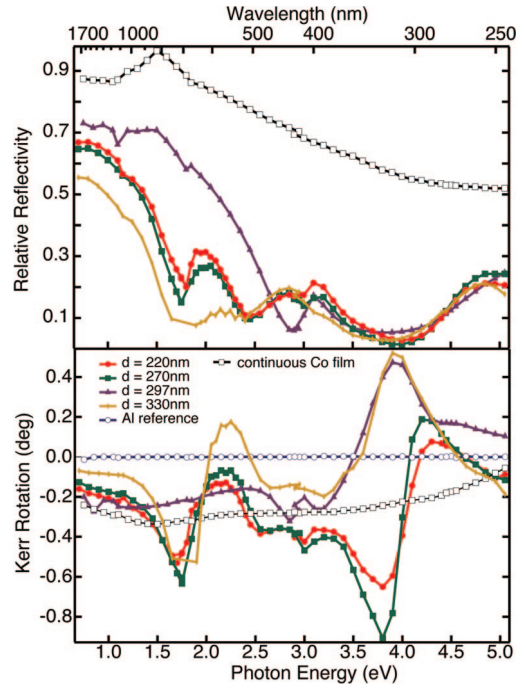
Figure 3. Relative reflectivity (upper graph) as well as magneto-optic Kerr measurements for four different Co hole diameters (full symbols). Additionally, the spectra for a continuous Co film are shown for comparison. The reflectivity is taken relative to the reflectivity of an aluminum mirror. The thickness of the metal film is for all measurements at 50 nm and the lattice parameter at 470 nm.

Changing the incident angle leaves the opportunity to measure the evolution of the transmission peaks along the Γ−K-direction of the hexagonal lattice. To compare the differences from the normal incident case, a spectrum taken at 20° incident angle is also plotted into Figure 2a (red squares). The spectrum looks now more complicated, having a number of additional peaks, while the main transmission maxima are red shifted, compared to their positions in the normal incident case. A map of the optical band structure for incident angles up to 30° along the Γ−K-direction is shown in Figure 2b where the evolution of the peaks can be followed. Additionally, the calculated dispersion of the different SP modes is included in the picture (dashed lines), which matches the measured dispersion very well. The lowest order modes for the film−substrate interface have been noted for assistance. Now, the spectrum for 20° incident angle in Figure 2a becomes clearer. The aforementioned red shift of the peaks is due to the dispersion of the SP modes. The evolution of peaks in positions where there were only minima at normal incidence is due to the dispersion of higher order modes. Thus, the mapped band structure can be completely described and understood by taking the dispersion of SP modes into account and shows that the structure supports SPs.

Figure 3 shows simultaneously recorded reflectivity and polar Kerr spectra for hole arrays with four different hole diameters but constant lattice parameter as well as a Co film without holes as the control sample. In contrast to the samples made for the transmission measurements, Si(111) was used in this case as substrate material, which changes the position

of the Wood anomalies as compared to the sapphire substrate. The reflectivity spectra of the different hole arrays (full symbols) show plasmonic resonances (minimum in reflectivity) similar to the optical transmission measurements shown in Figure 2a, while the continuous film shows the reflectivity of a metal (open squares). The spectra of the holes differ only slightly from each other and may be a result of slight differences in the quality of the sample surface. The main difference occurs between small, that is, 220 and 270 nm, and large, that is, 297 and 330 nm, hole diameters, yet the position of the majority of the peaks remains constant. These small changes, being apparent in the magnitude of the observed transitions, indicate the role of the hole diameter in the development of the spectrum since it is a direct measure of the filling fraction of the film (in our case ranging between 20 and 45%).

The lower graph in Figure 3 shows the recorded magneto-optic Kerr spectra. Again, for comparison, the spectra of the Al reference (open circles) as well as the control Co film (open squares) are inserted, showing the known features for the Co film: a negative Kerr rotation in the complete spectral range and the two broad minima at ~1.5 eV and ~4 eV, respectively. The magneto-optic response of the hole arrays is completely different from that of the Co film. There are a lot of maxima and minima visible for all hole-array samples from which the minimum at 1.75 eV, the maximum at 2.2 eV, and the peaks at 3.9 eV are the most pronounced, whereas the last one is also showing a change in the sign of the Kerr rotation. Since the continuous Co film does not exhibit such a complex spectrum, the visible structure has to be related to the hole array. Comparing the position of the peaks in the Kerr spectra with the transitions (minima) visible in the reflectivity spectra, it is evident that they are connected to each other. Since it is known[40] that there are optical enhancement effects in the magneto-optic spectra near a minimum in the reflectivity spectrum, the measured Kerr spectra are thus directly connected to the SP excitations of the hole array. A closer look at the spectra reveals differences between them. The most pronounced one is the structure at ~3.9 eV. For small holes, that is, 220 and 270 nm, there is a minimum only differing in the magnitude. For the larger holes, that is, 297 and 330 nm, there is a change in the sign of the Kerr rotation, and the samples show a maximum. We think that this drastic change is directly connected to the radius of the holes, since in this region the light's wavelength and the diameter of the holes are comparable.

As shown before, the hole array strongly influences the magnetic response of the Co film. To further study this influence, hysteresis curves have been measured in longitudinal (Figure 4a) as well as in polar (Figure 4b) Kerr geometry. Figure 4a shows the longitudinal Kerr hysteresis loops for the continuous Co film and for the samples with 220, 270, and 330 nm hole diameters, respectively, which have been recorded at a photon energy of 3.05 eV. As could be expected, the 50 nm thick continuous Co film displayed a uniaxial anisotropy with the easy axis of the magnetization lying in the film plane. The coercivity is about 2.5 mT, while the saturation field value is about 5 mT. For all hole-array
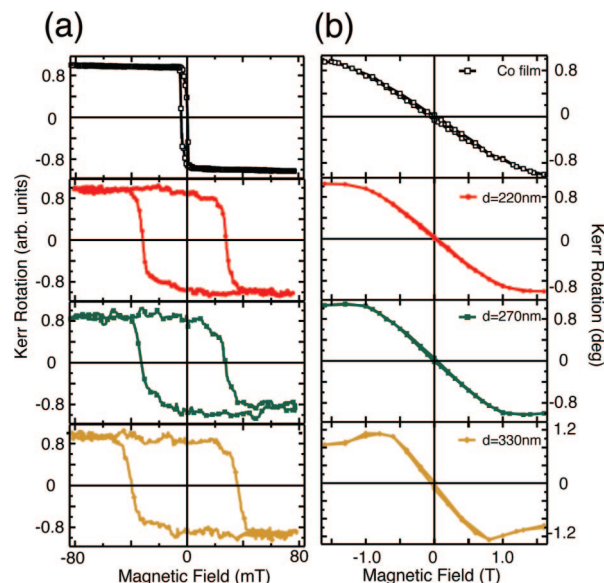

Figure 4. Measurement of hysteresis curves by means of magneto-optic Kerr effect (MOKE). (a) Longitudinal ($E = 3.05$ eV) and (b) polar ($E = 2.2$ eV) Kerr geometry.

samples, the measurements indicate that the easy axis of magnetization lies also in the film plane. However, the hysteresis loops indicate the dominant role of the holes in the reversal behavior over the intrinsic anisotropy of the cobalt film. The shape of the hysteresis curves is markedly modified by the presence of the nonmagnetic holes. Moreover, there is an increase in the coercive field as the hole size increases. The sample with the 330 nm holes exhibits the highest coercive field (38 mT). Commonly, the coercivity is found to increase with reduced interhole spacing (period) at fixed hole size[41] or with increasing hole size when the period is constant.[36] In our case, we have a different approach. We keep the interhole spacing constant at 470 nm while we change the hole size. The trend of magnetic hardening as the hole size increases can be explained if we consider that by increasing the hole size we increase at the same time the amount of the material that is ablated from the film, that is, for the $d = 330$ nm holes only ~46% of the total surface is covered with material. The latter imply that the influence of pinning sites (holes) is stronger to the films with less material. More pinning sites of the domain walls in the vicinity of the holes provide the observed increase in the coercivity. Preliminary micromagnetic simulations strengthen this explanation by showing an increase in coercive field with increasing hole diameter (not shown here). The increase in the coercivity in the in-plane geometry with increasing the hole size is followed by the opposite behavior in the out-of-plane geometry as Figure 4b reveals. Figure 4b displays the hysteresis curves for the different perforated films in the polar Kerr geometry at a photon energy of 2.2 eV. The curves affirm again that all samples have their hard axis out-of-plane. For the reference sample, the hysteresis loop shows a typical hard-axis behavior with no remanence and a saturation field of 1.45 T, being characteristic for a film with a uniaxial anisotropy. However, for the perforated films, the hysteresis loops are slightly modified. By increasing the hole size the saturation field decreases strongly (reaches
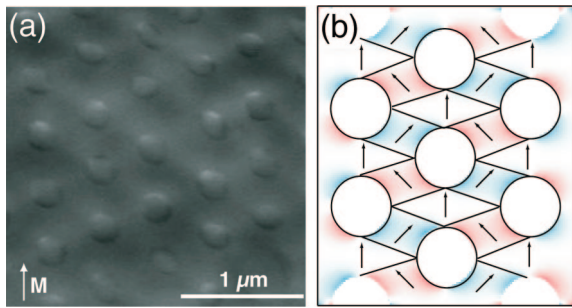
Figure 5. (a) MFM measurement of the 50 nm thick Co hole array with 270 nm hole diameter and an applied in-plane field of $B = 350$ mT. The direction of the magnetization is indicated in the figure. (b) Micromagnetic simulation of the situation measured in panel a. The color scale indicates the angle to the applied field direction (red: positive angle, blue: negative angle). For clarity, the domain situation is sketched into the picture indicating the influence of the holes on the domain formation in the film and being in good agreement to the MFM picture.

the value of 0.8 T for the sample with $d = 330$ nm), while a small remanence and coercivity appears. The behavior is consistent with Figure 4a and reveals the capability to modify the magnetization dynamics of the films through the hole pattern. The local dipolar fields introduced by the hole edges give rise to the out-of-plane components in competition with the intrinsic uniaxial anisotropy of the film. Besides, a surprisingly decrease in the magnetization after saturation is visible for the film with the 330 nm holes. The shape of the curve for this sample with the 330 nm holes indicates a possible ferromagnetic−antiferromagnetic exchange, maybe an effect of the cobalt−cobalt oxide interface, which is present at the hole sides. Measurements at different photon energies (not shown here) show no difference in the hysteresis curves. Only at a photon energy of 3.9 eV, the change in the sign as seen in the Kerr spectrum is also visible in the hysteresis measurement.

To further understand the influence of the hole array on the magnetic behavior of the Co film, magnetic force microscopy (MFM) was used to image possible domain formation. Figure 5a displays the recorded magnetic force image for an in-plane applied field of 350 mT in the direction as indicated by the arrow in the picture. The scan size is 2.5 × 2.5 μm^2. A nearly constant interaction is visible over the film. At the position of the holes stronger changes appear. On the one hole edge, attractive forces can be measured, while on the opposite edge, repulsive interaction is detected. The measured interactions point along the external field and thus along the film magnetization. An explanation is provided by the end domains at the hole edges along the field, which are responsible for the measured out-of-plane field components. In order to explain the microscopic distribution of the spin orientation, micromagnetic simulations have been performed, using an object-oriented micromagnetic framework (oommf) code from NIST.[42] The parameters used for the calculation are: saturation magnetization $M_S = 1.4 \times 10^6$ Am^{-1}, exchange constant $A = 30 \times 10^{12}$ Jm^{-1}, and an uniaxial anisotropy with an anisotropy constant of $K_{1,u} = 520 \times 10^3$ Jm^{-3}. To reduce computation time, a cell size of 10 nm was used. The convergence criterion was the

misalignment between magnetization and effective field ($|m \times h|$) to be lower than 10^{-5} in each computation cell. The thickness of the Co film was set to 50 nm. Figure 5b shows the result. It is easily seen that the average spin orientation is along the y-axis (along the applied field). Furthermore, there is one more set of spin orientations covering those spins having an angle of $\pm 30°$ to the y-axis. These domains are formed as a result of the shape anisotropy imposed by the two neighboring holes. In between the rhombohedral cell of the holes, the magnetization points along the magnetization direction. The calculated results agree well with the MFM-measurements and strengthen our assumption.

Summary and Outlook. In conclusion, we measured the optical and magneto-optic properties through a subwave-length hexagonal array of holes in a ferromagnetic cobalt film. The transmission through the perforated film is governed by the excitation of surface plasmons at the interfaces, which determine the position of the maxima as well as their evolution by changing the incident angle of the incoming light. The magneto-optic spectra show a complex structure with a higher polarization rotation than for the control Co film, being a direct result of an enhancement effect and closely related to the SP excitations, since their spectral position is given by the position of the SP maxima. The tuning of the magneto-optic behavior renders the system important for technological applications in magneto-optic data storage media, in magnetic photonic crystals, and in the new field of optoelectronics, since it leaves a further degree of freedom to manipulate light-matter interaction and thus control the propagation of light. The results of the MOKE magnetometry reveal the dominant role of the presence of the holes in the reversal behavior over the intrinsic anisotropy of the cobalt film and demonstrate the ability to control the coercivity of the films.

Further investigations concerning the transmission properties in the near-field, possible interactions between the surface plasmons and the film magnetization, as well as theoretical modeling are currently being prepared.

References
(1) Ebbesen, T. W.; Lezec, H. J.; Ghaemi, H. F.; Thio, T.; Wolff, P. A. *Nature* **1998**, *391*, 667.
(2) Ghaemi, H. F.; Thio, T.; Grupp, D. E.; Ebbesen, T. W.; Lezec, H. J. *Phys. Rev. B* **1998**, *58*, 6779.
(3) Kim, T. J.; Thio, T.; Ebbesen, T. W.; Grupp, D. E.; Lezec, H. J. *Opt. Lett.* **1999**, *24*, 256.
(4) Degiron, A.; Lezec, H. J.; Barnes, W. L.; Ebbesen, T. W *Appl. Phys. Lett.* **2002**, *81*, 4327.
(5) Barnes, W. L.; Dereux, A.; Ebbesen, T. W. *Nature* **2003**, *424*, 824.
(6) Klein Koerkamp, K. J.; Enoch, S.; Segerink, F. B.; van Hulst, N. F.; Kuipers, L. *Phys. Rev. Lett.* **2004**, *92*, 183901.
(7) Barnes, W. L.; Murray, W. A.; Dintinger, J.; Devaux, E.; Ebbesen, T. W. *Phys. Rev. Lett.* **2004**, *92*, 107401.
(8) van der Molde, K. L.; Segerink, F. B.; van Hulst, N. F.; Kuipers, L. *Appl. Phys. Lett.* **2004**, *85*, 4316.
(9) Dintinger, J.; Klein, S.; Bustos, F.; Barnes, W. L.; Ebbesen, T. W. *Phys. Rev. B* **2005**, *71*, 035424.
(10) Gao, H.; Henzie, J.; Odom, T. W. *Nano Lett.* **2006**, *6*, 2104.
(11) Kim, J. H.; Moyer, P. J. *Opt. Express* **2006**, *14*, 6595.
(12) Przybilla, F.; Degiron, A.; Laluet, J.-Y.; Genet, C.; Ebbesen, T. W. *J. Opt. A: Pure Appl. Opt.* **2006**, *8*, 458.
(13) Ctistis, G.; Patoka, P.; Wang, X.; Kempa, K.; Giersig, M. *Nano Lett.* **2007**, *7*, 2926.
(14) Genet, C.; Ebbesen, T. W. *Nature* **2007**, *445*, 39.

(15) Lesuffleur, A.; Im, H.; Lindquist, N. C.; Oh, S.-H. *Appl. Phys. Lett.* **2007**, *90*, 243110.

(16) Popov, E.; Nevière, M.; Enoch, S.; Reinisch, R. *Phys. Rev. B* **2000**, *62*, 16100.

(17) Krishnan, A.; Thio, T.; Kim, T. J.; Lezec, H. J.; Ebbesen, T. W.; Wolff, P. A.; Pendry, J.; Martín-Moreno, L.; García-Vidal, F. J. *Opt. Commun.* **2001**, *200*, 1.

(18) Martín-Moreno, L.; García-Vidal, F. J.; Lezec, H. J.; Pellerin, K. M.; Thio, T.; Pendry, J. B.; Ebbesen, T. W. *Phys. Rev. Lett.* **2001**, *86*, 1114.

(19) Sarrazin, M.; Vigneron, J.-P.; Vigoureux, J.-M. *Phys. Rev. B* **2003**, *67*, 085415.

(20) Lezec, H. J.; Thio, T. *Opt. Express* **2004**, *12*, 3629.

(21) Pendry, J. B.; Martín-Moreno, L.; García-Vidal, F. J. *Science* **2004**, *305*, 847.

(22) Chang, S.-H.; Gray, S. K.; Schatz, G. C. *Opt. Express* **2005**, *13*, 3150.

(23) García de Abajo, F. J.; Gómez-Medina, R.; Sáenz, J. J. *Phys. Rev. E* **2005**, *72*, 016608.

(24) Baida, F. I.; van Labeke, D. *Opt. Commun.* **2002**, *209*, 17.

(25) García; de Abajo, F. J. *Rev. Mod. Phys.* **2007**, *79*, 1267.

(26) Song, J. F.; Proietti Zaccaria, R. *J. Opt. A: Pure Appl. Opt.* **2007**, *9*, S450.

(27) Chern, R.-L. *Phys. Rev. B* **2008**, *77*, 045409.

(28) Rodrigo, S. G.; García-Vidal, F. J.; Martín-Moreno, L. *Phys. Rev. B* **2008**, *77*, 075401.

(29) Richard, R.; Dereux, A.; David, T.; Bourillot, E.; Goudonnet, J. P.; Scheurer, F.; Beaurepaire, E.; Garreau, G. *Phys. Rev. B* **1999**, *59*, 5936.

(30) Diwekar, M.; Kamaev, V.; Shi, J.; Vardeny, Z. V. *Appl. Phys. Lett.* **2004**, *84*, 3112.

(31) Foldyna, M.; Postava, K.; Ciprian, D.; Pištora, J. *J. Mag. Magn. Mater.* **2005**, *290−291*, 120.

(32) García-Martín, A.; Armelles, G.; Pereira, S. *Phys. Rev. B* **2005**, *71*, 205116.

(33) Belotov, V. I.; Doskolovich, L. L.; Zvezdin, A. K. *Phys. Rev. Lett.* **2007**, *98*, 077401.

(34) Zharov, A. A.; Kurin, V. V. *J. Appl. Phys.* **2007**, *102*, 123514.

(35) Przybilla, F.; Degiron, A.; Laluet, J.-Y.; Genet, C.; Ebbesen, T. W. *J. Opt. A: Pure Appl. Opt.* **2006**, *8*, 458.

(36) Heyderman, L. J.; Nolting, F.; Backes, D.; Czekaj, S.; Lopez-Diaz, L.; Kläui, M.; Rüdiger, U.; Vaz, C. A. F.; Bland, J. A. C.; Matelon, R. J.; Volkmann, U. G.; Fischer, P. *Phys. Rev. B* **2007**, *73*, 214429.

(37) Višňovský, Š.; Pařízek, V.; Nývlt, M.; Kielar, P.; Prosser, V.; Krishnan, R. *J. Magn. Magn. Mater.* **1993**, *127*, 135.

(38) (a) Rybczynski, J.; Ebels, U.; Giersig, M. *Colloids Surf., A* **2003**, *219*, 1. (b) Kosiorek, A.; Kandulski, W.; Chudzinski, P.; Kempa, K.; Giersig, M. *Nano Lett.* **2004**, *4*, 1359. (c) Kosiorek, A.; Kandulski, W.; Glaczynska, H.; Giersig, M. *Small* **2005**, *1*, 439.

(39) Raether, H. *Surface Plasmons*; Springer-Verlag: Berlin, 1998.

(40) Fumagalli, P.; Spaeth, C.; Rüdiger, U.; Gambino, R. J. *IEEE Trans. Magn.* **1995**, *31*, 3319.

(41) Wang, C. C.; Adeyeye, A. O.; Wu, Y. H. *J. Appl. Phys.* **2003**, *94*, 6644.

(42) Donahue, M. J.; Porter, D. G. oommf User's guide, Version 1.0, Interagency Report NISTIR 6376, National Institute of Standard and Technology, Gaithersburg, MD (1999): URL: http://math.nist.gov/oommf.